Melting of Tantalum at Multimegabar Pressures on the Nanosecond Timescale

R. G. Kraus,* F. Coppari, D. E. Fratanduono, R. F. Smith, A. Lazicki, C. Wehrenberg, and J. H. Eggert
Physics Division, Lawrence Livermore National Laboratory, Livermore, California 94550, USA

J. R. Rygg and G. W. Collins
Laboratory for Laser Energetics, and Departments of Mechanical Engineering and Physics and Astronomy,
University of Rochester, Rochester, New York 14627, USA

(Received 12 February 2021; accepted 5 May 2021; published 24 June 2021)

Tantalum was once thought to be the canonical bcc metal, but is now predicted to transition to the *Pnma* phase at the high pressures and temperatures expected along the principal Hugoniot. Furthermore, there remains a significant discrepancy between a number of static diamond anvil cell experiments and gas gun experiments in the measured melt temperatures at high pressures. Our *in situ* x-ray diffraction experiments on shock compressed tantalum show that it does not transition to the *Pnma* phase or other candidate phases at high pressure. We observe incipient melting at approximately 254 ± 15 GPa and complete melting by 317 ± 10 GPa. These transition pressures from the nanosecond experiments presented here are consistent with what can be inferred from microsecond gas gun sound velocity measurements. Furthermore, the observation of a coexistence region on the Hugoniot implies the lack of significant kinetically controlled deviation from equilibrium behavior. Consequently, we find that kinetics of phase transitions cannot be used to explain the discrepancy between static and dynamic measurements of the tantalum melt curve. Using available high pressure thermodynamic data for tantalum and our measurements of the incipient and complete melting transition pressures, we are able to infer a melting temperature 8070^{+1250}_{-750} K at 254 ± 15 GPa, which is consistent with ambient and a recent static high pressure melt curve measurement.

DOI: 10.1103/PhysRevLett.126.255701

Introduction.—The melt curve represents the largest rheological transition a material can undergo, from a material with strength to one without. The melt curve at high pressure is also an extremely sensitive test of our understanding of material behavior as the free energy surfaces of the high-temperature solid and liquid are nearly parallel. Unfortunately, for some materials there remains significant discrepancy in our experimental measurements of the high-pressure melt curve. Tantalum in particular still remains an enigma, where shock compression techniques and a single static high-pressure study find agreement along a high-temperature melt curve [1–3] while numerous other static high pressure experiments continue to measure a relatively low melting temperature [4–6].

Because of the tremendous experimental efforts on both sides of the argument, one must focus on performing robust experiments utilizing techniques that are least prone to systematic error. There is general agreement that robust detection of liquid is the predominant issue with melt curve measurements. While rapid recrystallization, sound speed changes, latent heat signatures, and reflectivity features have been used to detect melting, most widely accepted is the detection of diffuse liquid scattering within *in situ* x-ray diffraction experiments. However, detection of liquid with x-ray diffraction often requires long recording times at elevated temperatures, which can lead to chemical reactions that systematically lower the inferred melt temperature. Consequently, the optimal experiment would heat the sample faster than ionic diffusivity in the sample and then utilize *in situ* x-ray diffraction to detect liquid scattering. Given that the ionic diffusivity in the liquid is of order of 5×10^{-9} $\mathrm{m^2\,s^{-1}}$ [7], the heating timescale for few micrometer samples must be faster than a few hundred microseconds in order to ensure the sample is not permeated by material adjacent to the sample.

However, timescales this short lead to a new concern, which is that kinetics could cause the transition to occur at pressures or temperatures beyond those in equilibrium. Work by Refs. [8–10] and others suggest that shock wave measurements of melting, occurring on the microsecond timescale, need to be significantly corrected to lower temperatures to account for the degree of superheating expected. However, Luo *et al.* [11,12] analyzed the systematics of superheating signatures and concluded that superheating was insufficient to explain the discrepancy in experimental measurements in tantalum and other refractory metals, as was also found in the study by Ref. [13].

In this work, we experimentally constrain the melt curve of tantalum at high pressure and high temperature using a nanosecond x-ray diffraction measurement to ensure there is no time for significant chemical reactions. With *in situ* x-ray diffraction, we are able to directly observe the shock melting transition on the nanosecond timescale from a solid, to a mixed phase, to a pure liquid. To confirm that superheating is not significant, we compare these nanosecond dynamic compression experiments to previous microsecond dynamic compression experiments. We then use available thermodynamic data and our constraint on the shock melting transition pressures to infer the temperature on the high pressure melt curve of tantalum.

Experimental methods.—Nanosecond duration laser driven shock compression experiments were performed at the Laboratory for Laser Energetics at the University of Rochester on the OMEGA laser facility. Using a single beam of the Omega laser focused with a spot size of 800 μm diameter and using energies from 57 to 126 J, single steady shock waves were driven into the 38 μm thick Kapton Type HN ablator, which then transmitted the shock into the high purity, Goodfellows 99.9%, 8 μm thick tantalum foil samples, where the Kapton ablator was coated with 100 nm of aluminum to prevent shine through. When the shock wave is one-quarter to one-third of the way through the sample, 14 beams concurrently illuminate both sides of a 13 μm thick copper foil. These beams have a full width half maximum of 1 ns, and are focused down to 225 μm in diameter with energies from 200–250 J/beam. The plasma generated from this high energy laser emits He-α line radiation at 8.36 keV with a bandwidth of approximately 1%, with He-β line radiation at 9.86 keV at ~10% of the intensity of the He-α line [14]. Here a 300 μm diameter tantalum pinhole is used to collimate the x rays and the unshocked portion of the sample serves as a reference diffraction source, which enables accurate calibration of the location of the image plates relative to the sample and light source locations.

A schematic of the target used in these experiments and the diagnostic setup is shown in Fig. 1 where more details of the x-ray diffraction diagnostic, PXRDIP, is described in the work by Rygg *et al.* [15,16]. In these experiments, the uncertainty in the sample density determined by diffraction is propagated from the uncertainty in the 2θ angle of the (110) peak and the uncertainty in the x-ray source wavelength [14]. The pressure in the sample is determined by impedance matching the known Hugoniot of tantalum [17] and lithium fluoride (LiF)[18] using the measured velocity of the interface between the tantalum sample and the (100)-oriented LiF window using the line-imaging VISAR diagnostic [19,20]. The uncertainty in the pressure is obtained by standard error propagation through the impedance matching equations [21], with the inclusion of a systematic error associated with the slight nonsteadiness of the wave, which is discussed in the Supplemental Material [22].

Results.—Eight *in situ* diffraction experiments were performed, ranging from 201 to 343 GPa on the principal Hugoniot of tantalum. A summary of the experimental states achieved is shown in Table I. For shock pressures of 201 ± 9 and 243 ± 12 GPa, we observe a single textured diffraction peak from shocked tantalum; the (110) bcc line. The (200) peak at the shocked state is not observed in these experiments. The expected ratio of intensities in the (110) to (200) peak is ~5; if including the harmonic

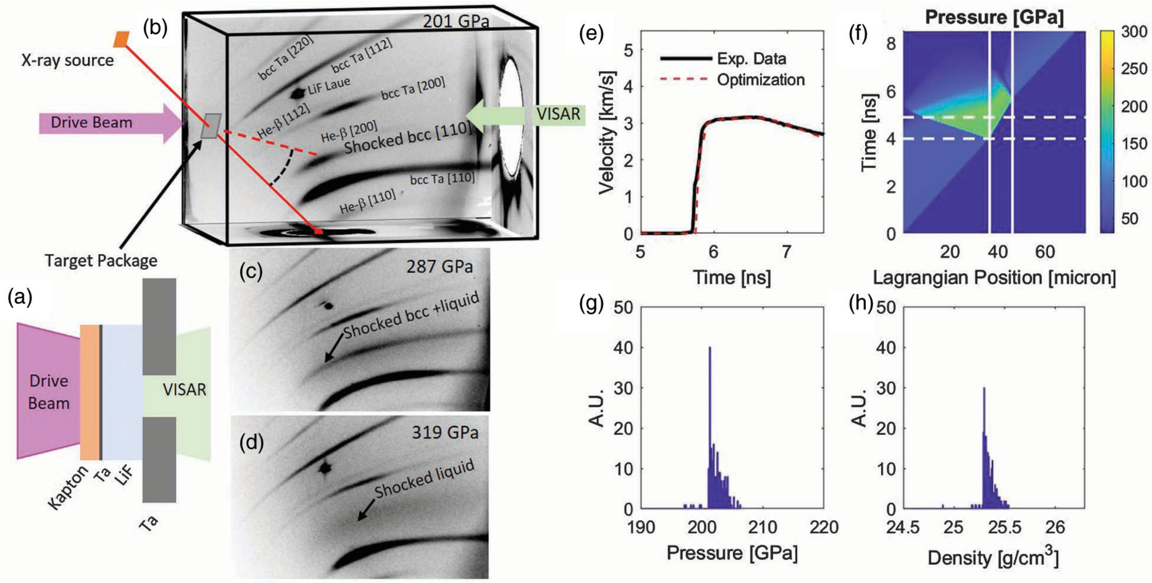

FIG. 1. Schematic of the target (a), diagnostic (b), including raw data from three experiments at pressures of 201 ± 9, 287 ± 15, and 319 ± 15 (b)–(d). A 50 mm hole is located on the PXRDIP box to allow for the line-VISAR diagnostic to measure the interface velocity at the tantalum-LiF interface. The VISAR data are used for direct impedance matching to determine the pressure of the shock in the tantalum, but also as input for a forward optimization (e) from which one can infer the pressure history in the sample (f), a pressure histogram at the time of x-ray exposure (g), and the expected density histogram (h).

TABLE I. Summary of the data observed in each experiment.

Experiment No.	Shock pressure [GPa]	Phase	Solid phase density [$\mathrm{g\,cm^{-3}}$]
75 280	201 ± 9	BCC	25.25 ± 0.15
75 293	243 ± 12	BCC	26.40 ± 0.22
75 284	264 ± 16	BCC + Liquid	27.27 ± 0.19
75 295	287 ± 15	BCC + Liquid	27.29 ± 0.31
75 282	311 ± 10	BCC + Liquid	27.24 ± 0.26
75 289	317 ± 11	Liquid	NA
75 291	319 ± 15	Liquid	NA
75 287	343 ± 17	Liquid	NA

Debye-Waller factor, this expected ratio increases to 10. In our experiments, the peak intensity of the (110) line at a given ϕ angle has a signal to noise ratio of ~60, however, because of texture, the minimum signal to noise ratio for the (110) peak falls to ~6. Consequently, because of a combination of texture and the Debye-Waller effect, we do not see the (200) or other higher order bcc diffraction lines.

A mixed-phase, partially molten state is first observed at a shock pressure of 264 ± 16 GPa, where the diffuse scattering feature is observable at the same scattering angle as the (110) peak of the solid component and the (110) peak has reduced in intensity by approximately a factor of 2 from the 243 GPa experiment. The diffuse scattering feature has a full width at half maximum 4 times greater than the solid component, increasing from 1.1° to 4.4°. The concurrent entrance of a broad diffuse scattering feature centered at the (110) peak of the BCC and the reduction of the intensity of the solid feature we take as evidence for the partial melting along the principal Hugoniot of tantalum. Similar mixed phase diffraction signatures are observed at shock pressures of 287 ± 15 and 311 ± 10. At shock pressures above 317 ± 11 GPa, there is a complete loss of the solid diffraction signature and only the diffuse liquid scattering feature is observed. These transitions can be clearly observed in the raw data, as seen in the image plate panels shown in Fig. 1. Lineouts of the dewarped x-ray diffraction data are shown in Fig. 2, where the profiles are offset for clarity.

In Fig. 3, we present the measured densities as a function of the shock pressure achieved in the sample, where the measured densities are in excellent agreement with the tantalum Hugoniot [17]. Also shown in Fig. 3 are the previous sound velocity measurements by Ref. [1] and Ref. [25] that are interpreted as signifying the melting transition. One can see that the slope changes in the sound velocity data occur at the same pressures of our experimentally measured incipient and complete melting transition pressures.

To test if the measured diffraction data could also be consistent with the *Pnma* structure, we evaluated the density of the shocked tantalum assuming the solid diffraction feature experimentally observed is the strongest line of the *Pnma* structures proposed in Refs. [9,26]. As shown in Fig. 3, the *Pnma* densities would not be consistent with the measured tantalum Hugoniot, where the uncertainty in the tantalum Hugoniot density and diffraction density measurement is ~1% and the *Pnma* phase density deviates by 4%–6%. There are more recent suggestions by Ref. [27] of alternative energetically favorable phases, such as *Cmcm*, *Fddd*, and *Pmma*. As shown in Fig. 4, these three structures share a strong diffraction peak with BCC at the same crystal density and hence cannot be immediately discarded due to density; however, they are also predicted to have strong diffraction lines at two-theta angles that are within the range observable of the PXRDIP and would not be expected to be sufficiently damped by the Debye-Waller effect. Consequently, we conclude that tantalum melts along the principal Hugoniot from the bcc phase.

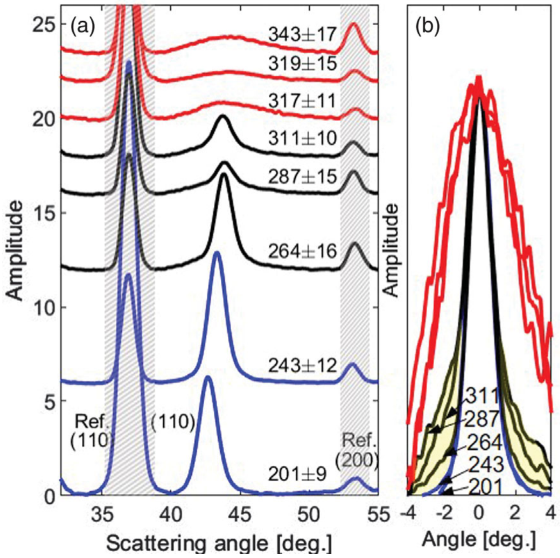

FIG. 2. Diffraction lineouts show the transition from sharp solid diffraction (blue) to broad liquid diffraction (red) with a coexistence (black) at intermediate pressures. (a) Lineouts from the image plates are offset for clarity. Also included are the hkl indices of the shocked data and the reference pinhole lines, hatched regions, as well as the associated pressures in GPa for each lineout and estimated uncertainty. (b) Line-shape comparison of the scattering feature from the shocked tantalum, where all lines are centered at 0° and are scaled to the same peak amplitude. The onset of melting can be seen in the black lineouts in how they deviate from the blue lineouts, highlighted by the shaded yellow region.

Discussion.—As in the work of Ref. [1], we do not measure temperature in these shock wave experiments, but we do accurately determine the internal energy change from the ambient to the shocked state through the Rankine-Hugoniot equation. With some bounded assumptions for the electronic contribution to the heat capacity, [1] predicted the temperature for incipient melting using available thermodynamic data, although they incorrectly interpreted the complete loss of shear strength as the incipient melting

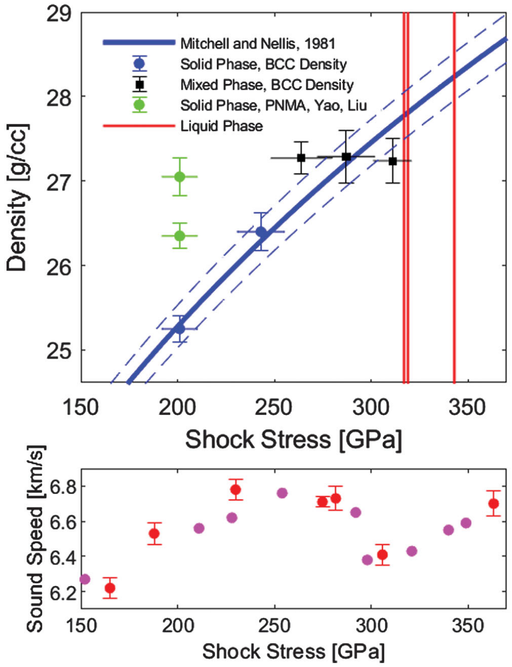

FIG. 3. Top: Measured density of the solid phase observed in each diffraction experiment assuming the phase is bcc. The tantalum Hugoniot [28] is shown in the solid blue line with uncertainties bounds as dashed blue lines. At the lowest pressure experiment, shown in green are two interpretations of the diffraction data if the first strong diffraction peak is inferred to be due to the *Pnma* phase [9,26]. The pressures at which liquid diffraction data are observed are shown with the red vertical lines. Bottom: Sound velocity data of tantalum from [1] magenta and [25] red.

transition and not the complete melting transition. With the more recent shock temperature measurements of Ref. [2], Hugoniot measurements [17], isothermal compression measurements [29], and our measurements of the incipient and complete melting transition pressure, we have developed an experimentally constrained equation of state model for tantalum, with more details provided in the Supplemental Material [22]. Shown in Fig. 5 is our predicted Hugoniot along with uncertainties; which are based upon bounding the shock temperature data from Ref. [2] while forcing the incipient melting transition to occur at 254 GPa and completing at 315 GPa as determined from our diffraction data (marked along the Hugoniot).

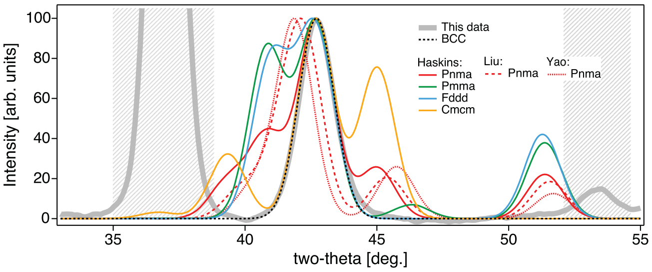

FIG. 4. Comparison of experimental diffraction data with recently proposed structures for the high temperature phases of tantalum by [9,26,27], where the diffraction patterns are calculated with the approximate instrumental resolution of the PXRDIP diagnostic,~1.6° FWHM, at the density on the Hugoniot of tantalum at 200 GPa, 25.25 $\mathrm{g\,cm^{-3}}$ and photon wavelength of 1.483 angstroms. Hatched vertical bands represent regions where the reference pinhole lines dominate the diffraction pattern.

At 254(15) GPa, we find a melt temperature of 8070(+1250, −750) K. The consistency between the ambient melt temperature and slope, the high pressure melt curve measurements of Ref. [3], and our inferred shock melt temperature suggests the dynamic and static high pressure communities are converging to the same answer. Adding confidence to the interpretation of our dynamic compression experiments is that the slope of the melt curve as predicted by the latent heat signature along the Hugoniot is in excellent agreement with the Simon fit, $T = 3293(P/185.5 + 1)^{1.04}$.

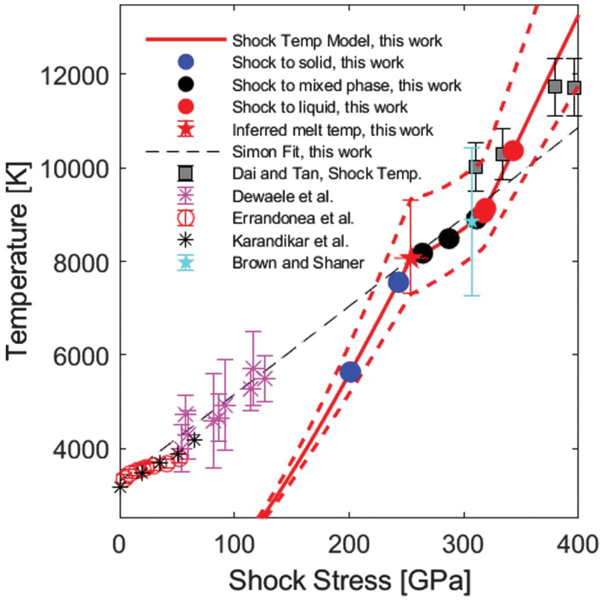

FIG. 5. The temperature along the Huognt and its uncertainty, red solid and dashed lines, is constrained by the shock temperature measurements by [2], gray squares, with more details provided in the Supplemental Material [22]. The phases observed at a given pressure along the Hugoniot—solid, mixed, and liquid—are plotted at the calculated temperature, using large filled blue, black, and red circles, respectively. From the calculated shock temperatures, we infer a high pressure melting temperature at the pressure for incipient melting determined here, red star. This high pressure melt datum and ambient pressure melt datum is fit to the Simon melt equation, black dashed line, which is compared to the static melt curve measurements of Refs. [3–6]. Also compared is the previous dynamic compression sound speed measurement of Ref. [1], where temperature is calculated using a similar thermodynamic model but without the constraints of temperature data from Ref. [2].

Alternatively, if the discrepancy between extrapolations of static measurements of the tantalum melt curve, Refs. [4,5], and the dynamic compression measurements shown here are interpreted to be solely due to kinetics, as discussed in Refs. [8,9], the overdriving pressure for the melting transition would need to be > 80 GPa. This hypothesis is inconsistent with the agreement between these nanosecond x-ray diffraction results and the microsecond timescale sound velocity experiments [1,25], ∼10 GPa. Furthermore, our observation of a two-phase region is also inconsistent with the hypothesis that the melt curve is overdriven by 80 GPa in dynamic compression experiments, as the excess enthalpy in overdriving the transition would be more than sufficient to completely melt the material as soon as the melt phase first nucleates, and one would never observe a mixed phase. Finally, we note that our observation cannot be interpreted as metastable melting of bcc at high temperature with equilibrium melting occurring at lower temperature from the *Pnma* structure because thermodynamics requires that the stable phase must have a higher melting temperature than a metastable melt curve.

Conclusions.—Here we present *in situ* x-ray diffraction measurements of tantalum shocked from ∼200 to 350 GPa. With increasing shock pressure, we observe the transition from bcc tantalum, to a mixed phase of bcc and liquid at 254 ± 15 GPa, to completely liquid tantalum at 317 ± 10 GPa. Proposed alternative structures of tantalum are not observed at the high temperatures and pressures in this work, providing confidence that BCC is the stable high temperature phase. The transition pressures observed in these nanosecond timescale experiments are compared to the incipient and complete melting transition pressures observed in microsecond timescale gas gun experiments, and we find them to be in excellent agreement. The degree of experimental agreement between these significantly disparate timescale experiments and the observation of a mixed phase itself suggests that kinetics of melting is insufficient to explain the discrepancy in some static and dynamic compression experiments for measuring the melting curve of tantalum. With our accurate characterization of the melting transition pressures along the Hugoniot, we are able to use the shock temperatures of Dai *et al.* [2] to infer a high pressure melting temperature and slope that are consistent with both ambient data and recent static high pressure data by Dewaele *et al.* [3], which provides confidence that we are converging on the true high pressure melt curve of tantalum.

We acknowledge the target fabrication efforts of C. Davis and support at the Laboratory for Laser Energetics by C. Sorce, N. Whiting, and J. Tellinghuisen. This work was performed under the auspices of the U.S. Department of Energy by Lawrence Livermore National Laboratory under Contract DE-AC52-07NA27344.

[*]Corresponding author.
kraus4@llnl.gov

[1] J. Brown and J. Shaner, Rarefaction velocities in shocked tantalum and the high-pressure melting point, in *Proceedings of the American Physical Society Shock Compression of Condensed Matter* (North-Holland Physics Publishing, Amsterdam, 1983), https://doi.org/10.1016/B978-0-444-86904-3.50022-1.

[2] C. Dai, J. Hu, and H. Tan, Hugoniot temperatures and melting of tantalum under shock compression determined by optical pyrometry, J. Appl. Phys. **106**, 043519 (2009).

[3] A. Dewaele, M. Mezouar, N. Guignot, and P. Loubeyre, High Melting Points of Tantalum in a Laser-Heated Diamond Anvil Cell, Phys. Rev. Lett. **104**, 255701 (2010).

[4] D. Errandonea, B. Schwager, R. Ditz, C. Gessmann, R. Boehler, and M. Ross, Systematics of transition-metal melting, Phys. Rev. B **63**, 132104 (2001).

[5] D. Errandonea, M. Somayazula, D. Hausermann, and H. K. Mao, Melting of tantalum at high pressure determined by angle dispersive x-ray diffraction in a double-sided laser heated diamond-anvil cell, J. Phys. Condens. Matter **15**, 7635 (2003).

[6] A. Karandikar and R. Boehler, Flash melting of tantalum in a diamond anvil cell to 85 GPa, Phys. Rev. B **93**, 054107 (2016).

[7] L. Vocadlo, D. Alfe, G. D. Price, and M. J. Gillan, First principles calculations on the diffusivity and viscosity of liquid Fe-S at experimentally accessible conditions, Phys. Earth Planet. Interiors **120**, 145 (2000).

[8] D. Errandonea, Improving the understanding of the melting behaviour of Mo, Ta, and W at extreme pressures, Physica (Amsterdam) **357B**, 356 (2005).

[9] C. M. Liu, C. Xu, Y. Cheng, X. R. Chen, and L. C. Cai, Melting curves and structural properties of tantalum from the modified-z method, J. Appl. Phys. **118**, 235901 (2015).

[10] R. Hrubiak, Y. Meng, and G. Shen, Microstructures define melting of molybdenum at high pressures, Nat. Commun. **8**, 14562 (2017).

[11] S. N. Luo, T. J. Ahrens, T. Cagin, A. Strachan, W. A. Goddard, and D. C. Swift, Maximum superheating and undercooling: Systematics, molecular dynamics simulations, and dynamic experiments, Phys. Rev. B **68**, 134206 (2003).

[12] S. N. Luo and T. J. Ahrens, Shock-induced superheating and melting curves of geophysically important minerals, Phys. Earth Planet. Interiors **143–144**, 369 (2004).

[13] J. Wang, F. Coppari, R. Smith, J. Eggert, A. Lazicki, D. Fratanduono, J. Rygg, T. Boehly, G. Collins, and T. Duffy, X-ray diffraction of molybdenum under shock compression to 450 GPa, Phys. Rev. B **92**, 174114 (2015).

[14] F. Coppari, R. F. Smith, D. B. Thorn, J. R. Rygg, D. A. Liedahl, R. G. Kraus, A. Lazicki, M. Millot, and J. H. Eggert, Optimized x-ray sources for x-ray diffraction measurements at the omega laser facility, Rev. Sci. Instrum. **90**, 125113 (2019).

[15] J. R. Rygg, J. H. Eggert, A. E. Lazicki, F. Coppari, J. A. Hawreliak, D. G. Hicks, R. F. Smith, C. M. Sorce, T. M. Uphaus, B. Yaakobi, and G. W. Collins, Powder diffraction

from solids in the terapascal regime, Rev. Sci. Instrum. **83**, 113904 (2012).

[16] J. R. Rygg *et al.*, X-ray diffraction at the National Ignition Facility, Rev. Sci. Instrum. **91**, 043902 (2020).

[17] A. C. Mitchell and W. J. Nellis, Shock compression of aluminum, copper, and tantalum, J. Appl. Phys. **52**, 3363 (1981).

[18] P. A. Rigg, M. D. Knudson, R. J. Scharff, and R. S. Hixson, Determining the refractive index of shocked [100] lithium fluoride to the limit of transmissibility, J. Appl. Phys. **116**, 033515 (2014).

[19] L. M. Barker and R. E. Hollenbach, Shock-wave studies of pmma, fused silica, and sapphire, J. Appl. Phys. **41**, 4208 (1970).

[20] P. M. Celliers, G. W. Collins, L. B. Da Silva, D. M. Gold, and R. Cauble, Accurate measurement of laser-driven shock trajectories with velocity interferometry, Appl. Phys. Lett. **73**, 1320 (1998).

[21] J. Asay and M. Shahinpoor, *High-Pressure Shock Compression of Solids* (Springer-Verlag, New York, 1993).

[22] See Supplemental Material at http://link.aps.org/supplemental/10.1103/PhysRevLett.126.255701 for detailed information about determining the shock pressure and temperature, which includes Refs. [23,24].

[23] S. J. Ali, R. G. Kraus, D. E. Fratanduono, D. C. Swift, and J. H. Eggert, An iterative forward analysis technique to determine the equation of state of dynamically compressed materials, J. Appl. Phys. **121**, 195901 (2017).

[24] D. C. Wallace, *Statistical Physics of Crystlas and Liquids* (World Scientific, Singapore, 2002).

[25] M. Akin, J. Nguyen, M. Beckwith, R. Chau, W. Ambrose, O. Fatyanov, P. Asimow, and N. Holmes, Tantalum sound velocity under shock compression, J. Appl. Phys. **125**, 145903 (2019).

[26] Y. Yao and D. D. Klug, Stable structures of tantalum at high temperature and high pressure, Phys. Rev. B **88**, 054102 (2013).

[27] J. B. Haskins and J. Moriarty, Polymorphism and melt in high-pressure tantalum. II. Orthorhombic phases, Phys. Rev. B **98**, 144107 (2018).

[28] A. Mitchell and W. J. Nellis, Shock compression of aluminum, copper, and tantalum, J. Appl. Phys. **52**, 3363 (1981).

[29] A. Dewaele, P. Loubeyre, and M. Mezouar, Equations of state of six metals above 94 GPa, Phys. Rev. B **70**, 094112 (2004).